Self-Consistent Analysis of Carrier–Transport and Carrier–Capture Dynamics in Quantum Cascade Intersubband Semiconductor Lasers

K. Kálna, C. Y. L. Cheung, I. Pierce, and K. A. Shore, *Senior Member, IEEE*

***Abstract*—A methodology for the self-consistent analysis of carrier transport and carrier capture aspects of the dynamics of quantum cascade intersubband semiconductor lasers is described in this paper. The approach is used to analyze two prototype quantum cascade lasers. The self-consistent analysis incorporates the calculation of the electron densities and temperatures in each subband, together with the intersubband relaxation time. In the calculation of the relaxation time, we take into account the electron interaction with polar optical and acoustic phonons, as well as electron degeneracy. In addition, we also calculate the capture time, considering backward processes that play a role in the electron transition from an injection into an active region. The calculations indicate intersubband relaxation times of order 1 ps and capture times of order 100 fs.**

***Index Terms*—Dynamic response, infrared lasers, quantum-well devices, semiconductor heterostructures, semiconductor lasers.**

I. Introduction

THIS PAPER describes a theoretical framework for performing calculations of the fundamental time constants that determine the dynamics of carrier transport and carrier capture in intersubband quantum cascade semiconductor lasers. Intersubband lasers have become a topic of active research, particularly following the development by Faist *et al.* of mid-infrared (MIR) quantum cascade lasers [1], which was the first practical demonstration of a long-standing proposal for the utilization of intersubband transitions to obtain lasing action in semiconductor superlattices [2]. Subsequent research at AT&T, Lucent Technologies [3], [4], and in a growing number of laboratories across the U.S. and Europe has given rise to significant developments in the performance of quantum cascade lasers. In this context, it is of considerable interest to examine the dynamic behavior of quantum cascade lasers with a view, in particular, for evaluating the achievable direct current modulation bandwidth of such lasers. It is noted that the picosecond carrier lifetimes, which are characteristic of the operation of intersubband lasers, may be anticipated to offer opportunities for terahertz bandwidth modulation in such lasers. This aspect has been previously investigated where use was made of a rate equation model described in [5] and [6] to derive expressions for the modulation response of unipolar semiconductor lasers [7]. Subsequent work [8] has generalized that approach to yield a self-consistent rate equation analysis where, in particular, carrier lifetimes are deduced from calculations of electronic wave functions in the structure. Reference [8] indicated that modulation bandwidths of an order of 150 GHz would be obtainable in the chosen structure.

In a recent report [9], it was indicated that unipolar lasers have the potential for achieving terahertz modulation bandwidths, and a detailed description of that analysis has been presented elsewhere [10]. This literature was concerned with the dynamical processes occurring in a single triple-quantum-well (QW) element. In practical intersubband lasers, in order to achieve sufficient optical gain, the active region must contain many copies of such elements so as to achieve the quantum cascade effect, which underpins the successful operation of this class of lasers. In order to analyze the dynamical processes at play in such a quantum cascade laser, attention needs to be given to carrier–transport and carrier–capture processes, which will affect, in particular, the achievable direct current modulation frequency of intersubband cascade lasers. In this paper, a theoretical framework will be established to perform calculations of the pertinent physical factors that govern carrier transport.

In this paper, the generic structure that is assumed to form the building block of the active layer of the electrically pumped intersubband laser of interest is as shown in Fig. 1, i.e., a coupled triple-QW element with an injector well, a central laser well, and an extractor well denoted by QW numbers 1–3, respectively. In general, the carrier transport between the wells is characterized by a tunneling time τ_{12} describing injection from QW 1 to 2—the lasing well—and a tunneling time τ_{23} from the lasing well to QW 3—the extractor well. As shown in previous studies [5]–[8], the laser dynamics is further determined by the carrier transit time through the structure τ_T and the intersubband relaxation time τ_S. The essence of this study is to perform a calculation of the relevant carrier lifetimes with a view to determining the dynamical properties of quantum cascade lasers.

A quantum cascade laser can be considered as being constructed from a series "cascade" of coupled QW structures of the kind illustrated schematically in Fig. 1. In order to describe the dynamical processes in a single element of such a structure, in Fig. 1 we introduce a notation for identifying the energy levels and carrier populations in those levels: subscripts identify the QW number and superscripts identify the energy subband level. As far as an isolated element is concerned, an

Manuscript received March 1, 1999; revised July 13, 1999. This work was supported by the Royal Society.

K. Kálna is with the Institute of Electrical Engineering, Slovak Academy of Sciences, 842 39 Bratislava, Slovakia.

C. Y. L. Cheung, I. Pierce, and K. A. Shore are with the Bangor School of Electronic Engineering and Computer Systems, University of Wales, Bangor LL57 1UT, Wales, U.K.

Publisher Item Identifier S 0018-9480(00)02521-7.

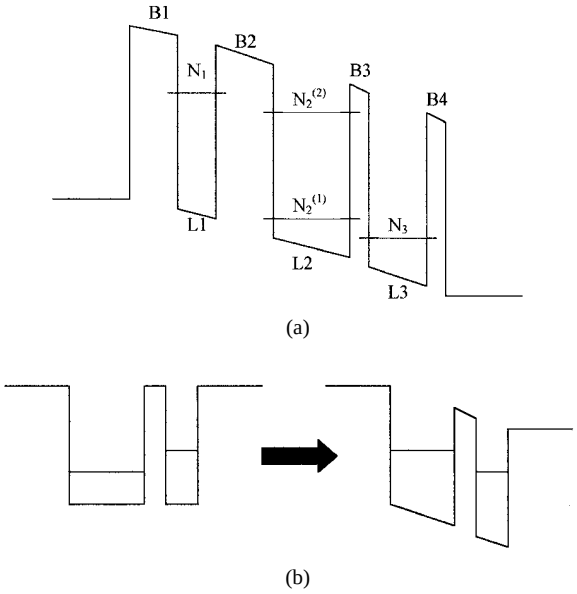

Fig. 1. Schematic diagram of the conduction band of the triple-QW intersubband GaAs/$Al_{0.45}Ga_{0.55}As$ laser structure, with well widths of 2.9, 8.2, and 6.0 nm, respectively, and barrier widths of 4.0, 5.0, 3.0, and 2.4 nm, respectively.

electron can be considered to enter the structure by tunneling through the first barrier B1 to the energy level E_1 in the first QW, i.e., W1. Tunneling through to $E_2^{(2)}$ in the second QW, i.e., W2, it then makes a vertical transition to $E_2^{(1)}$, after which it rapidly tunnels to E_3 in the third QW, i.e., W3, and escapes out of the structure. In order to achieve this, the four lowest energy levels are such that we have one each localized in W1 (E_1) and W3 (E_3), and two localized in W2 ($E_2^{(1)}$ and $E_2^{(2)}$), when the structure is in an unbiased condition. At an appropriate bias voltage, coupling occurs between E_1 and $E_2^{(2)}$, and between $E_2^{(1)}$ and E_3.

The dynamics of such a single cell have been examined in some detail in previous work [5]–[9]. The aim of this paper is to study the modifications in predicted dynamical response that arise due to the effects of interelement carrier transport and the finite time associated with the capture of electrons in the well structure. Calculations will thus be performed for the structure described in [7] and [8], where our analysis is based on a structure that is designed for operation at a lasing wavelength of nominally 10 μm, thus, the lasing transition should have an energy of more or less 124 meV. In order to achieve this, it is assumed that a suitable bias voltage is applied to the structure, such that the separation between the two energy levels involved in the transition is of this value.

The framework for analysis developed here is of general applicability, but for the sake of definiteness in prescribing the salient physical processes that are required for accurately predicting the response, this study concerns structures fabricated in the GaAs/AlGaAs system. This material system offers an advantage in terms of the well-advanced state of information concerning fundamental material constants. A recent report [12] of the successful demonstration of intersubband lasing in this material system provides particular motivation for analyzing this structure.

TABLE I
ELECTRON SHEET DENSITIES AND TEMPERATURES OBTAINED FROM SELF-CONSISTENT CALCULATIONS FOR THE STRUCTURE OF FIG. 1

Energy level	Sheet density [$\times 10^{14}$ m^{-2}]	Temperature [K]
E_1 (W1)	1.91	93.3
$E_2^{(2)}$ (W2)	1.29	98.5
$E_2^{(1)}$ (W2)	1.11	109.1
E_3 (W3)	0.48	109.5
Intersubband time	1.07 ps	

II. CHARACTERISTIC LIFETIMES

A. Tunneling Times

The tunneling time τ_{ij} is defined as the time that it takes for an electron to travel from one side of the barrier in one well to the other side of the barrier in the next well, assuming that both wells are coupled together. It is determined by the energy separation between the eigenenergies ΔE_{ij} of the coupled wells such that

$$\tau_{ij} = \frac{\pi\hbar}{\Delta E_{ij}}. \tag{1}$$

Thus, in order to have a fast escape time from W2, the separation between $E_2^{(1)}$ and E_3 should be as large as possible without losing coupling between W2 and W3. This energy separation ΔE_{ij} is related to the coupling strength between the coupled wells, which, in turn, is strongly affected by the height and thickness of the barrier in between the wells, and the width of the wells. The stronger the coupling strength between the wells, the larger is the possible energy separation [11], resulting in a faster tunneling time through the barrier.

B. Wave Function and Lifetime Calculations

We use the argument principle method (APM) described in [8] to perform calculations of the wave functions and lifetimes of the proposed structure and find that, when biased to 75 meV, the structure eigenenergies and corresponding state lifetimes are as shown in Table I. The APM is a method of solving for the complex zeros of an analytical function, which, in this case, consists of the time-independent effective-mass Schrödinger equation, which has as solutions the eigenenergies and electron lifetimes of the structure. Their respective wave functions (Fig. 2) show coupling between W1 and W2, and between W2 and W3, as required.

III. ANALYSIS TECHNIQUE

The rate equations for carrier densities [see (2)–(6)] as well as the rate equations for energy densities [see (8)–(11)] depend on the intersubband relaxation time τ_S and on the capture time τ_{12}. Both the rate equations give the electron volume density N_i and temperature T_{ei} in the ith energy subband. These two quantities enter back into the calculations of the electron relaxation times. Hence, it is natural to calculate the electron densities, temperatures, and relaxation times self-consistently until the convergence is retained. An iteration process starts with the rate equations for carrier densities and continues with the rate equations for energy densities and, finally, the relaxation time is calculated. The whole process is then repeated. Fortunately, these

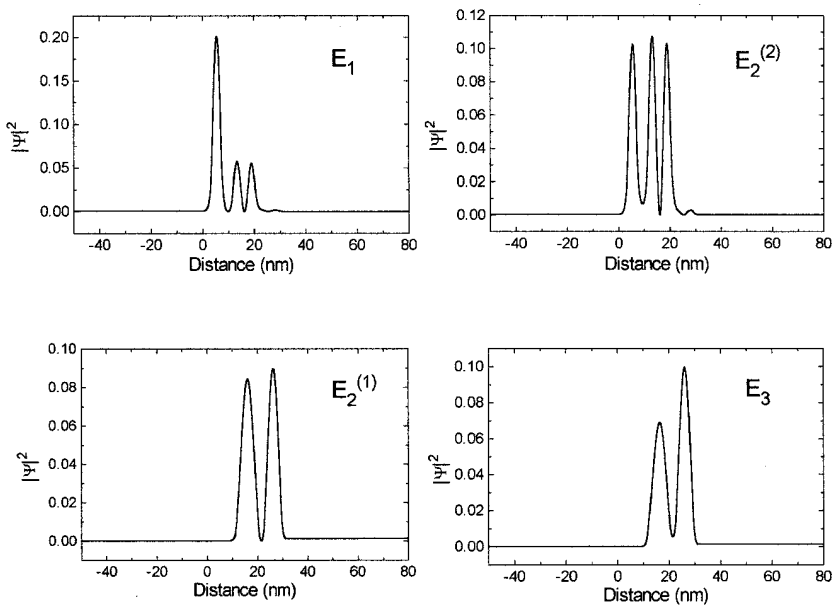

Fig. 2. Wave functions of the energy levels for the structures of Fig. 1. The applied bias is 75 meV.

iterations converge rather fast, usually taking no more than five cycles or so. When that convergence is obtained, an evaluation of the capture time is performed using the carrier densities and temperature obtained from the self-consistent calculations. The self-consistency may be further enhanced by incorporating the calculation of the capture time within the iteration loop. This, however, significantly increases the computation time and, for the present, this has not been undertaken. It is observed that the calculated capture time has a very reasonable value.

A. Carrier Dynamics

The following rate equations are applicable to four-level three-well structures with a vertical lasing transition in well W2 between the subbands $N_2^{(2)}$ and $N_2^{(1)}$, as illustrated in the structure shown in Fig. 1:

$$\frac{dN_1}{dt} = \frac{J}{eL_1} + \frac{L_2 N_2^{(2)}}{L_1 \tau_{12}} - \frac{N_1}{\tau_{12}} \tag{2}$$

$$\frac{dN_2^{(2)}}{dt} = \frac{L_1 N_1}{L_2 \tau_{12}} - \frac{N_2^{(2)}}{\tau_{12}} - aP(N_2^{(2)} - N_2^{(1)}) - \frac{N_2^{(2)}}{\tau_S} \tag{3}$$

$$\frac{dN_2^{(1)}}{dt} = aP(N_2^{(2)} - N_2^{(1)}) + \frac{N_2^{(2)}}{\tau_S} + \frac{L_3 N_3}{L_2 \tau_{23}} - \frac{N_2^{(1)}}{\tau_{23}} \tag{4}$$

$$\frac{dN_3}{dt} = \frac{L_2 N_2^{(1)}}{L_3 \tau_{23}} - \frac{N_3}{\tau_{23}} - \frac{J}{eL_3} \tag{5}$$

$$\frac{dP}{dt} = aP(N_2^{(2)} - N_2^{(1)}) - \frac{P}{\tau_P} \tag{6}$$

where e is the electronic charge, a is the local gain coefficient, P is the photon density, and L_i is the width of the ith well. τ_{12} and τ_{23} are the tunneling times between W1 and W2 and between W2 and W3, respectively, calculated previously, as shown in [8]. τ_S is the intersubband relaxation time and τ_P is the photon lifetime.

Since the current injection is equal to the rate of total charge passing through the resonant tunneling QW structure, we can write

$$J = \frac{e}{\tau_T}\left[N_1 L_1 + \left(N_2^{(1)} + N_2^{(2)}\right)L_2 + N_3 L_3\right] \tag{7}$$

where τ_T is the effective transit time of the carriers through the whole structure, which includes not only the tunneling times through the barriers and the intersubband transition times, but also the time delays caused by intrasubband scattering and electron diffusion. J is the biasing current density.

B. Carrier Temperature Dynamics

The carrier temperature dynamics can be modeled using the intersubband energy density equations corresponding to the structure, following Willatzen's model for interband lasers [13]

$$\frac{dU_1}{dt} = \frac{N_2^{(2)}\langle E_{21}\rangle}{L_1\tau_{12}} - \frac{N_1\langle E_{12}\rangle}{\tau_{12}} + \frac{J\langle E_{p,2}\rangle}{eL_1} - \frac{U_1 - U_{L,1}}{\tau_{\text{heat}}} \tag{8}$$

$$\frac{dU_2^{(2)}}{dt} = -aP(N_2^{(2)} - N_2^{(1)})E_{c2} - \frac{U_2^{(2)}}{\tau_S} + \frac{L_1 N_1\langle E_{12}\rangle}{L_2\tau_{12}} - \frac{N_2^{(2)}\langle E_{21}\rangle}{\tau_{12}} - \frac{U_2^{(2)} - U_{L,2}^{(2)}}{\tau_{\text{heat}}} \tag{9}$$

$$\frac{dU_2^{(1)}}{dt} = aP(N_2^{(2)} - N_2^{(1)})E_{c1} + \frac{U_2^{(2)}}{\tau_S} + \frac{L_3 N_3\langle E_{43}\rangle}{L_2\tau_{23}} - \frac{N_2^{(1)}\langle E_{34}\rangle}{\tau_{23}} - \frac{U_2^{(1)} - U_{L,2}^{(1)}}{\tau_{\text{heat}}} \tag{10}$$

$$\frac{U_3}{dt} = \frac{N_2^{(1)}\langle E_{34}\rangle}{L_3\tau_{23}} - \frac{N_3\langle E_{43}\rangle}{\tau_{23}} + \frac{J\langle E_{p,1}\rangle}{eL_3} - \frac{U_3 - U_{L,3}}{\tau_{\text{heat}}} \tag{11}$$

where $\tau_{\rm heat}$ is the thermalization time towards the equilibrium energy density $U_{L,i} = U_i(N_i, T_L)$ and is assumed to be the same for all subbands. $E_{p,2}$ is the difference in energy between the electrons coming into the structure and the energy level in W1, while $E_{p,1}$ is the difference in energy between the electrons leaving the structure and the energy level in W3, and $E_{c,i}$ are the quasi-Fermi levels of the upper and lower lasing subbands. E_{ij} denotes the energy difference in electrons coming from subband i to subband j. Only electrons coming in from a higher subband are assumed to contribute to the energy of a subband. Finally, U_i gives the energy density in the ith subband and

$$U_i = \int dE\, E\, \rho(E)\, f_i(E) \tag{12}$$

where $\rho(E)$ is the density of states function in a QW and $f_i(E)$ is the Fermi distribution function for the ith subband.

In the model presented above, free carrier absorption has been neglected.

C. Intersubband Optical Gain

In previous work, we have performed calculations of optical gain in intersubband lasers [14]. Here, we outline the approach taken. Starting from the general standard expression for optical gain per meter in a semiconductor [15], we find that

$$g(\hbar\Omega) = \frac{\pi e^2\hbar}{n\epsilon_0 m_0^2}\frac{1}{\hbar\Omega}|M_T(E_{21})|^2\rho_r(E_{21})\int dE_{12}(f_2 - f_1) \cdot L(\hbar\omega_0 - E_{21}) \tag{13}$$

where $|M_T(E_{21})|$ is the transition matrix element, $\rho_r(E_{21})$ is the reduced density of states, $L(h\nu_0 - E_{21})$ is the line-shape function, andm_0 is the electron rest mass. The density of states for a QW $\rho_r(E_{21}) = (m_r/\pi\hbar^2 W)$, where W is the QW width. The transition matrix element is occasionally written as the dipole moment matrix element and the relationship between the two is given by $|M_T(E_{21})|^2 = m_0^2\Omega^2|z|^2$. We will be using the dipole moment matrix element

$$g(\hbar\Omega) = \frac{e^2|z_{12}|^2 m_r\Omega}{\hbar^2 cn\epsilon_0 W}\int_0^\infty d\epsilon \frac{\hbar\gamma(\epsilon).\left[f_2(\epsilon) - f_1(\epsilon)\right]}{\pi\left[\hbar\Omega - \hbar\Omega_\epsilon\right]^2 + \left[\hbar\gamma(\epsilon)\right]^2} \tag{14}$$

which is similar to the expression given in [16] and [17], except that (14) above is in MKS units and has the reduced effective subband mass m_r, Ω_ϵ is the optical transition frequency for the in-plan electron momentum, $\hbar k = \sqrt{2m_2\epsilon}$, $\hbar\Omega_\epsilon \equiv \hbar\Omega_0 + \epsilon_2 - \epsilon_1$, where $\hbar\Omega_0$ is the lasing energy at $k = 0$, $\epsilon_2 \equiv \epsilon$ and $\epsilon_1 = \hbar^2k^2/2m_1$ are kinetic energies in the upper and lower lasing subbands, respectively, characterized by the effective masses m_1 and m_2, and the distribution functions f_1 and f_2. Hence, the reduced mass $m_r = m_1m_2/(m_1 + m_2)$. The function $\gamma(\epsilon)$ describes the transverse phase relaxation due to intrasubband scattering [16].

In [17], it was assumed that $\gamma(\epsilon)$ is dominated by the interaction with polar optical phonons (pop's), such that

$$\gamma(\epsilon) = \gamma_0 \times \begin{cases} N_{\boldsymbol{q}} \\ (N_{\boldsymbol{q}} + 1)\theta(\epsilon - \hbar\omega) \end{cases} \tag{15}$$

where the top line describes optical phonon absorption and the bottom line describes optical phonon emission

$$\gamma_0 = \frac{\pi e^2}{2\hbar}\left(\frac{1}{\kappa_\infty} - \frac{1}{\kappa}\right)q, \qquad q = \sqrt{2m\omega/\hbar}.$$

The phonon distribution function $N_{\boldsymbol{q}}$ is Bose distribution in the following form:

$$N_{\boldsymbol{q}} = \left[\exp\left(\frac{\hbar\omega}{k_B T_L}\right) - 1\right]^{-1} \tag{16}$$

where T_L is the lattice temperature and k_B is the Boltzmann constant. The phonon frequency ω in the case of pop's is dispersionless ($\omega = \omega_{\rm pop}$). $\theta(\epsilon - \hbar\omega_{\rm pop})$ is a step function, κ and κ_∞ are the static and high-frequency dielectric constants, respectively, and m is the electron effective mass.

IV. Electron Relaxation Times

Electron relaxation dynamics in the intersubband lasers are governed predominantly by the electron interaction with pop's. Nevertheless, in order to verify its contribution, we have also taken into account, via the deformation potential interaction, electron scattering by acoustic phonons. Both phonons are considered to be bulk-like because incorporation of some phonon-confined model affects the overall results to a degree (<10%) comparable to other fine effects such as nonparabolicity [18].

The electron–phonon rates are calculated using Fermi's golden rule as a transition from the initial subband i with energy E_i to the final subband j with energy E_j. The electron rate with an initial energy E can then be obtained for the pop scattering as [19], [20]

$$\Gamma_{ij}^{\rm PO\pm}(E) = \frac{e^2\omega_{\rm pop}m}{8\pi\hbar^2}\left(\frac{1}{\kappa_\infty} - \frac{1}{\kappa}\right)\int_0^{2\pi} d\theta \cdot \left(N_{\boldsymbol{q}} + \frac{1}{2} \pm \frac{1}{2}\right)\frac{F_{iijj}(q)}{q} \tag{17}$$

where the pop wave vector is

$$q = \frac{\sqrt{2m}}{\hbar}\left(2E - E_{\rm PO} - 2\sqrt{E}\sqrt{E + E_{\rm PO}}\cos\theta\right)^{1/2} \tag{18}$$

with $E_{\rm PO} = E_i - E_j \mp \hbar\omega_{\rm pop}$. In (17) and (18), the upper sign stands for the phonon emission, while the lower sign stands for the phonon absorption.

The form factor F_{iijj}, which plays a crucial role in the rate (17), is defined by

$$F_{iijj}(q) = \int_{-\infty}^{\infty} dz_1 \int_{-\infty}^{\infty} dz_2\chi_i(z_1)\chi_j(z_2)e^{-q|z_1 - z_2|} \cdot \chi_j^*(z_1)\chi_j^*(z_2) \tag{19}$$

with the electron wave functions $\chi_i(z_1)$ and $\chi_j(z_2)$ obtained using the APM method [8].

The relaxation rate of an electron with initial energy E scattered by acoustic phonons reads

$$\Gamma_{ij}^{\rm AC\pm} = \frac{D^2 m}{8\pi\hbar^2\rho v_S}\int_0^{2\pi} d\theta\left(N_{\boldsymbol{q}} + \frac{1}{2} \pm \frac{1}{2}\right)q^2 F_{iijj}(q) \tag{20}$$

where the acoustic phonon wave vector is

$$q = \frac{\sqrt{2m}}{\hbar}\left(2E - E_{\rm AC} - 2\sqrt{E}\sqrt{E+E_{\rm AC}}\cos\theta\right)^{1/2} \quad (21)$$

with the elastic equipartition approximation given by $E_{\rm AC} = E_i - E_j$ [19]. Since the lattice temperatures T_L in our intersubband lasers are sufficiently high ($T_L \geq 77$ K), the equipartition approximation works very well.

In (20) and (21) for the electron rate, D is the acoustic deformation potential, ρ is the mass density, and v_S is the velocity of sound in the material. The phonon frequency ω in the case of acoustic phonons can be approximated by the linear dispersion relation as $\omega = v_S q$. Note here that only the deformation potential interaction has been taken into account for the electron-acoustic phonon scattering because the piezoelectric interaction is even weaker and, therefore, can be neglected [21].

The capture and intersubband relaxation times are sums of the averaged electron intersubband rates

$$\frac{1}{\tau} = \sum_i \frac{1}{N_{Si}} \sum_j \int_0^\infty \cdot dE \left\{ f_i(E)\Big[1 - f_j(E')\Big]\Big[\Gamma_{ij}^{+}(E) + \Gamma_{ij}^{-}(E)\Big] - \Big[1 - f_i(E')\Big] f_j(E)\Big[\Gamma_{ji}^{-}(E) + \Gamma_{ji}^{+}(E)\Big] \right\} \quad (22)$$

where

$$\Gamma_{ij}^{\pm} = \Gamma_{ij}^{\rm PO\pm} + \Gamma_{ij}^{\rm AC\pm} \quad (23)$$

N_{Si} represents the sheet electron density in the ith subband, and the electron final energy $E' = E + E_{\rm PO}$ or $E' = E + E_{\rm AC}$, respectively. The electron distribution functions f_i and f_j are taken as Fermi distributions

$$f_\alpha(E) = \left[\exp\left(\frac{E + E_\alpha - F_\alpha}{k_B T_{e\alpha}}\right) + 1\right]^{-1}, \qquad \alpha = i, j. \quad (24)$$

In (24), $T_{e\alpha}$ is the electron temperature and F_α is a quasi-Fermi energy, both in the αth subband. The quasi-Fermi energy F_α is a function of the electron temperature and the sheet electron density, which are obtained from rate equations in the following section.

The summations over initial states i and over final states j in (22) depends on whether capture or relaxation processes are being considered. In the case of the capture time τ_{12}, the sum over i involves all subbands in the injection region as well as the lowest subband of the previous active region. The sum over j involves all upper subbands in the active region. In the case of the intersubbband relaxation time τ_S, the first sum goes over all upper subbands and the second one over all lower subbands in the active region only. Further, the second term in (22) does not contribute to the overall sum because the backward processes are negligible in this case. Screening of the electrons is not involved in both of the rates of (17) and (20) because it is greatly reduced for intersubband scattering [22], especially where the sheet electron densities in the particular subbands are up to 2×10^{10} cm^{-2}.

V. Results and Discussion

Using the above quantities, the self-consistency scheme described in the previous section is utilized to perform calculations of the salient features of the laser dynamics. Results presented here are for the lifetimes calculated self-consistently for the structure of Fig. 1, while for the lifetimes of the structure described in [12], we have been used the parameters given in [12].

The electrons in the upper subband levels in the structures of Fig. 1 have high enough sheet densities to achieve a population inversion and, consequently, to participate in laser action. The sheet density in the highest energy subband (E_1) is also largest. Therefore, we expect that transitions from this level to the lower ones are the most effective. The electron sheet densities in the middle QW indicate that electron transitions between these levels are not as effective as from E_1. The electron temperatures increase with decrease in the subband energies. We have found an intersubband relaxation time of 1.07 ps after the self-consistent calculations. Further, we have calculated the capture time to be 0.28 ps using the self-consistent results for the electron densities and temperatures. It has been noted in Section III that the capture time was not included in the self-consistent scheme. Performing this calculation self-consistently requires significant additional computation time.

For the structure of [12], we have found a relaxation intersubband time of 4.0 ps at the temperature equal to 77K. The corresponding state lifetimes τ_1, τ_2, and τ_3 in the active region (see [12, Fig. 1] are 0.97, 0.67,and 0.60 ps, respectively. The relaxation intersubband time calculated by us is about two times larger than that of [4], but we believe that our calculations more accurately consider such processes as tunneling between the wells, acoustic phonon interactions, electron degeneracy, and includes also the applied bias. The population inversion conditions $\tau_S - \tau_2 > 0$ and $\tau_S - \tau_1 > 0$ are even better satisfied in our case. We have also calculated a capture time of 1.8 ps for the structure in [12]. This time, which represents an efficiency of the electron capture from the injection region into the active region, is short enough to encourage the rebuilding of the electron population inversion in the upper level.

The tunneling time τ_{23} has also been calculated and found to have an unusually high value of 6.6 ps. This is because the energy difference between levels 2 and 3 is less than the pop energy. In fact, if one wants to find the tunneling time more exactly, the transitions into the following injection region should also be taken into account.

The results obtained here can be used, for example, in order to ascertain the direct-current modulation response of such lasers. Such work is currently in progress.

Acknowledgment

One of the authors, K. Kálna, is very grateful for the kind hospitality from the Royal Society during his stay at the University of Wales, Bangor, U.K. Helpful discussions with Dr. P. Rees, Bangor, U.K., are also gratefully acknowledged.

References

[1] J. Faist, F. Capasso, D. L. Sivco, C. Sirtori, A. L. Hutchinson, and A. Y. Cho, "Quantum cascade laser," *Science*, vol. 264, pp. 553–556, 1994.

[2] R. F. Kazarinov and R. A. Suris, "Possibility of the amplification of electromagnetic waves in a semiconductor with a superlattice," *Soviet Phys.—Semicond.*, vol. 5, p. 797, 1971.
[3] J. Faist, F. Capasso, D. L. Sivco, C. Sirtori, A. L. Hutchinson, and A. Y. Cho, "Continuous wave operation of a vertical transition quantum cascade laser above $T = 80$ K," *Appl. Phys. Lett*, vol. 67, no. 21, pp. 3057–3059, 1995.
[4] C. Sirtori, J. Faist, and F. Capasso *et al.*, "Mid-infrared (8.5 μm) semiconductor lasers operating at room temperature," *IEEE Photon. Technol. Lett.*, vol. 9, pp. 294–296, Mar. 1997.
[5] W. M. Yee, K. A. Shore, and E. Schöll, "Carrier transport and intersubband population inversion in coupled quantum wells," *Appl. Phys. Lett.*, vol. 63, no. 8, pp. 1089–1091, 1993.
[6] W. M. Yee and K. A. Shore, "Threshold current density calculations for far-infrared semiconductor lasers," *Semicond. Sci. Technol.*, vol. 9, pp. 1190–1197, 1994.
[7] C. Y. L. Cheung, P. S. Spencer, and K. A. Shore, "Modulation bandwidth optimisation for unipolar intersubband semiconductor lasers," *Proc. Inst. Elect. Eng.*, vol. 144, no. 1, pp. 44–47, 1997.
[8] C. Y. L. Cheung and K. A. Shore, "Self-consistent analysis of the direct-current modulation response of unipolar semiconductor lasers," *J. Mod. Opt.*, vol. 45, no. 6, pp. 1219–1229, 1998.
[9] N. Mustafa, L. Pesquera, C. Y. L. Cheung, and K. A. Shore, "THz bandwidth prediction for amplitude modulation response of unipolar intersubband semiconductor lasers," *IEEE Photon. Technol. Lett.*, vol. 11, pp. 527–529, May 1999.
[10] ——, "Theoretical analysis of small-signal modulation bandwidth of unipolar intersubband semiconductor lasers," IEEE Trans. Microwave Theory Tech., submitted for publication.
[11] J. H. Smet, C. G. Fonstad, and Q. Hu, "Intra and interwell intersubbans transitions in multiple quantum wells for far-infrared sources," *J. Appl. Phys.*, vol. 79, pp. 9305–9320, 1996.
[12] C. Sirtori, P. Kruck, S. Barbieri, P. Collot, J. Nagle, M. Beck, J. Faist, and U. Oesterle, "GaAs, $Al_xGa_{1-x}As$ quantum cascade lasers," *Appl. Phys. Lett.*, vol. 73, no. 24, pp. 3486–3488, 1998.
[13] M. Willatzen, A. Uskov, J. Mørk, H. Olesen, B. Tromborg, and A.-P. Jauho, "Nonlinear gain suppression in semiconductor lasers due to carrier heating," *IEEE Photon. Technol. Lett.*, vol. 3, no. 7, pp. 606–609, July 1991.
[14] C. Y. L. Cheung, P. Rees, and K. A. Shore, "Gain calculations for unipolar semiconductor lasers," *Proc. Inst. Elect. Eng.*, vol. 146, pp. 9–13, 1999.
[15] L. A. Coldren and S. W. Corzine, *Diode Lasers and Photonics Integrated Circuits*. New York: Wiley, 1995, ch. 4.
[16] B. Gelmont, V. B. Gorfinkel, and S. Luryi, "Theory of spectral lineshape and gain in quantum wells with intersubband transitions," *Appl. Phys. Lett.*, vol. 68, no. 16, pp. 2171–2173, 1996.
[17] V. B. Gorfinkel, B. Gelmont, and S. Luryi, "Theory of gain spectra for quantum cascade lasers and temperature dependence of their characteristics at low and moderate carrier concentrations," *IEEE J. Quantum Electron.*, vol. 32, pp. 1995–2003, Nov. 1996.
[18] D. F. Nelson, R. C. Miller, and D. A. Kleinman, "Band nonparabolicity effects in semiconductor quantum wells," *Phys. Rev. B., Condens. Matter*, vol. 35, no. 14, pp. 7770–7772, 1987.
[19] B. K. Ridley, *Quantum Processes in Semiconductors*, 3rd ed. Oxford, U.K.: Clarendon, 1993.
[20] S. M. Goodnick and P. Lugli, *Hot Carriers in Semiconductor Nanostructures*, J. Shah, Ed. New York: Academic, 1992, p. 191.
[21] D. K. Ferry, *Semiconductors*. New York: Macmillian, 1991, p. 217.
[22] M. Dür, S. M. Goodnick, and P. Lugli, "Monte Carlo simulation of intersubband relaxation in wide, uniformly doped $GaAs/Al_xGa_{1-x}As$ quantum wells," *Phys. Rev. B., Condens. Matter*, vol. 54, no. 24, pp. 17–794, 1996.

K. Kálna, photograph and biography not available at time of publication.

C. Y. L. Cheung, photograph and biography not available at time of publication

I. Pierce, photograph and biography not available at time of publication

K. A. Shore (M'88–SM'95), photograph and biography not available at time of publication